Intrinsic Time- and Wavelength-Resolved Fluorescence of Oligonucleotides: A Systematic Investigation Using a Novel Picosecond Laser Approach

Regina Plessow, Andreas Brockhinke,* Wolfgang Eimer, and Katharina Kohse-Höinghaus

Physikalische Chemie I, Fakultät für Chemie, Universität Bielefeld, Universitätsstr. 25, D-33615 Bielefeld, Germany

Received: November 22, 1999

A novel picosecond laser approach is used to investigate the intrinsic fluorescence of several oligonucleotides. All biomolecules are excited at 283 nm with laser pulses of typically 80 ps duration and an energy of 250 μJ; concentrations were on the order of 10^{-5} M. Detection of the resulting fluorescence behind a spectrometer with a streak camera permits the simultaneous acquisition of spectral and lifetime information in two-dimensional images. In a systematic study, the fluorescence spectra and the associated temporal decays are analyzed with respect to monomer and potential excimer components. For this, the nucleotides AMP, CMP, GMP, and TMP are studied as well as homo-oligonucleotides of the type $d(X)_n$ with variable sequence length of $n = 2-15$, enabling a comparison of the emission characteristics of these single-stranded compounds under physiologic conditions in solution at room temperature. Also, the influence of conformational changes on the fluorescence response is investigated using mixtures of complementary oligonucleotides $d(X)_{15}\times d(Y)_{15}$ with the combinations X = A, Y = T and X = G, Y = C. These structures, which form double helices, differ in flexibility and stacking geometry from the single-stranded compounds. From experiments with self-complementary variants with alternating base sequences of the type $d(XY)_8$ with XY = AT and GC, information on exciplex formation tendencies is obtained for these compounds, which also form double helices in solution. Preliminary results of time-dependent fluorescence anisotropy measurements with this direct picosecond laser approach are discussed.

Introduction

The analysis of the three-dimensional structure of biomolecules and of their dynamic behavior in solution under biologically relevant conditions is one of the key topics of research in biochemistry and molecular biology. In this regard, much interest has been directed towards the study of DNA and related biopolymers. DNA flexibility is of great importance for many processes, including packaging in the chromosomes, protein recognition, and interaction with drugs which may intercalate between the double helix.[1] Also, more localized information on conformational dynamics, e.g. including base pair opening[2] or base pair mismatch,[3] may be desired with respect to point mutations, formation of photodefects, and DNA repair. Investigations of the internal dynamics of DNA rely on only a few, but powerful analytical tools, namely NMR, EPR, and fluorescence studies. For the latter, fluorescence labeling is often performed with suitable dyes and fluorophores,[4] the most common of which may be ethidium bromide.[5−7] This and other fluorescent labels, including pyrene,[8,9] fluorescein,[10,11] rhodamine,[12] and novel dyes[13−16] have proven of immense value not only in studies of structural and dynamic aspects but also in DNA sequencing,[13,14] fluorescence assays,[17] fluorescence microscopy,[16−18] capillary electrophoresis,[13−19] and flow cytometry.[20,21] With regard to the time-dependent structural properties of native DNA, dyes might not leave the system under study unchanged.[22] Even fluorescent probes with large structural similarities to some of the DNA building blocks such as 2-aminopurine,[17−23] which exhibits a much larger quantum yield than its close relative adenine, or N-6,N-6 dimethyladenosine or TNP-ATP[24] as an adenosine derivative may not show similar emission characteristics.[23,25]

Intrinsic DNA fluorescence thus has important advantages for the study of internal dynamic aspects since the three-dimensional structure and its flexibility and motion remain those of the native system. The photophysics of DNA has been studied for more than 3 decades, a major reason for this being the sensitivity of DNA and RNA to UV light and the desire to understand photoinduced damage to biological material.[26−31] For the aromatic nature of the nucleobases, DNA constituents exhibit surprisingly low quantum yields,[1,29] and the first studies of DNA and the related bases, nucleosides, and nucleotides had to be performed at low temperatures to enable detection of their native fluorescent emission.[26,27,32−34] Subsequent investigations on various model systems and native DNA arrived at measuring the static excitation and emission behavior in solution at room temperatures.[35−38] However, some of the information obtained at different temperatures was discussed controversially[28,37,39] with respect to spectral features at long wavelengths and the contribution of triplet states to the emission. Time-dependent fluorescence studies were awaited to resolve some of the open questions.

Although quite a few articles on lifetime and quenching issues for DNA and related molecules have appeared since the first direct picosecond study in 1984,[40] the emission lifetimes from the first excited singlet state for individual nucleic acid bases and some nucleosides and nucleotides were only reported from a systematic study about 2 years ago,[41] some of the results being in conflict with earlier literature.[31] A reason for the obvious

* Corresponding author. Phone: (49) 521 106 2189. Fax: (49) 521 106 6027. E-mail: brockhinke@pc1.uni-bielefeld.de.

10.1021/jp994132u CCC: $19.00 © 2000 American Chemical Society
Published on Web 03/23/2000

experimental difficulties are the extremely short lifetimes of these biomolecules in the picosecond regime, which require stable short-pulse UV laser sources and appropriate detection methods. Several techniques have provided time-resolved fluorescence information on DNA and related compounds.

Time-resolved fluorescence anisotropy enables the direct observation of base motion in DNA, which occurs on a picosecond time scale;[3] here, 2-aminopurine has been used as internal fluorescent label. Fluorescence excited with a mode-locked cavity-dumped dye laser was detected with a photomultiplier, and a histogram of photon detection times was constructed for two emission polarization directions. For similar purposes, commercial phase-shift fluorimeters are being used for dynamic fluorescence anisotropy measurements relying on ethidium bromide as a fluorescence label.[6,7] Georghiou et al.[1] state that there was a complete lack of polarized intrinsic fluorescence time-resolved studies of nucleic acids until 1996. In their own work, they have used a single-photon counting technique for fluorescence detection at 360 nm after excitation at 293 nm with a 1 ps synchronously pumped dye laser; typical sample concentrations were on the order of $10^{-3}-10^{-4}$ M. Pump-and-probe methods, employing laser pulses of picosecond[31] and femtosecond[42] duration, have been used to reconstruct the temporal development of the fluorescence emission by varying the delay between pump and probe pulse. However, this is often only feasible at a single[31] or a few[42] emission wavelengths, so detailed spectral information is lost. It appears that there are almost no direct picosecond fluorescence studies on DNA and its building blocks which provide fluorescence spectra as well as temporal decays, an exception being the early study of Kobayashi et al.[40] on adenine and polyadenylic acid. A combination of these two parameters—wavelength and time dependence—is greatly desirable in view of the potential contribution of excimers to the fluorescence emission. Also, a systematic comparison of the photophysics of mono-, di-, and polynucleotides with time- and wavelength-resolved fluorescence is still lacking.

In the present study, we have therefore chosen a novel approach using amplified picosecond laser radiation which allows one to simultaneously record the spectral and temporal fluorescence behavior in two-dimensional images. Using this method, we have studied time- and wavelength-resolved fluorescence of the individual nucleotides AMP, CMP, GMP, and TMP. We have then investigated the influence of adjacent bases of the same kind by varying the sequence length in single-stranded oligonucleotides of the configuration $d(X)_n$, with X = A, C, G, T and $n = 2-15$. This allows for the first time an intercomparison of excimer formation tendencies for homologous oligonucleotides of a given sequence length. This information is complemented with investigations of oligonucleotide mixtures which form double helices as well as with self-complementary oligonucleotides of the same length featuring alternating base sequences. Exciplex formation tendencies and conformational aspects will be discussed as a consequence of these experiments. The potential of the present equipment for the study of polarized time- and wavelength-resolved fluorescence will be shown in demonstration experiments.

Experimental Arrangement

The laser and detection arrangement is shown schematically in Figure 1. The laser system (Spectra Physics) consists of a Ti:sapphire laser (Tsunami) pumped by a 7 W Ar^+ laser. It is capable of producing pulses with 3 ps and 80 ps duration. The selection of the pulse duration is done with a Gires-Tournois

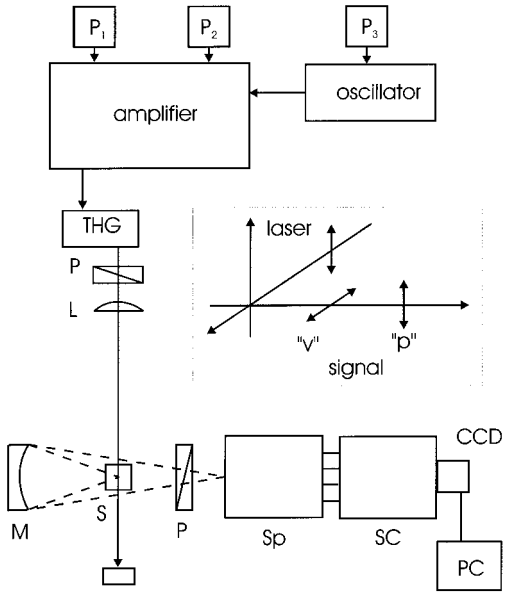

Figure 1. Experimental setup. The oscillator is a mode-locked Ti: sapphire laser. S, sample; CCD, detector camera; L, lens; M, mirror; P, polarizer; P_1, Ar^+ pump laser; P_2, P_3, Nd:YAG pump laser; PC, computer; SC, streak camera; Sp, spectrograph; THG, frequency tripling unit. The insert shows the geometry of laser and signal polarization directions.

interferometer; wavelength selection is performed with a birefringent filter consisting of three parallel quartz plates. In this configuration, the laser emits pulse trains in the near-infrared (between 750 and 900 nm) with a repetition frequency of 82 MHz, and individual pulses have an energy of approximately 10 nJ. For the present application, 80 ps pulses with considerably higher energy in the UV were desired. For this, three amplification stages and several frequency conversion processes are needed. A regenerative amplifier (TSA-50) and two linear amplifiers are used; they are pumped with the second harmonic radiation of two Nd:YAG lasers. With amplification factors of 10^5, 2.5, and 4, respectively, the resulting pulses at about 850 nm have typical energies of 15 mJ and a repetition rate of 10 Hz. Consecutive frequency-doubling and mixing of the second harmonic with the fundamental wavelength provides UV radiation near 283 nm with a pulse length of 80 ps, pulse energy of 250 μJ, and bandwidth of about 0.7 cm^{-1}. The temporal shape of the pulse is obtained with an autocorrelator, and the wavelength position is controlled with a dual-bandwidth wavemeter (Burleigh).

Samples were contained in quartz cuvettes of 10×10 mm^2 (Hellma type 111-QS, Suprasil, optical precision) and positioned reproducibly in the laser beam with a special receptacle. The laser radiation was not centered through the cuvette but directed closer to one of the sides. Also, emission was detected close to where the laser had entered the cuvette. Both measures served to minimize loss of intensity and reabsorption of emitted radiation.

The fluorescence emission was collected with a spherical mirror ($f = 250$ mm, $d = 250$ mm) to avoid chromatic aberrations when using a large spectral detection range. A cutoff filter (Schott WG 320, 3 mm) at 320 nm was used to block Rayleigh scattering and scattered light from optical surfaces. The emission was spectrally dispersed with a 27.5 cm imaging spectrometer (Acton Research Corp., SpectraPro 275i) which is equipped with different gratings. In these experiments, two gratings with a dispersion of 600 and 150 g mm^{-1} were used, spanning a wavelength range of 48 and 200 nm, respectively.

Temporal resolution was achieved with a streak camera (Hamamatsu C2830), the output of which was amplified, imaged on a phosphor screen, and coupled to a CCD camera (C4880), where the data were stored and transmitted to a computer. The image detected by the streak camera was a size of 1000 × 1018 pixels, and it was decoded by the HPD-TA software supplied by Hamamatsu. The time interval may be selected to be 0.5, 1, 2, 5, and 10 ns; the temporal scale of the resulting images then corresponds to 4060 ps (5 ns) and 7860 ps (10 ns), respectively. For the detection of time-dependent polarization effects, a Glan prism was used in front of the spectrometer. To enhance the vertical polarization, a Rochon prism was added in this case.

Samples were prepared with tridistillated water and p.a. grade chemicals if not stated otherwise. A Tris/EDTA buffer (10 mM tris, 0.1 mM EDTA, 150 mM NaCl) with a pH of 7.1 and a physiologic salt concentration is used as solvent. Oligonucleotides were purchased from Midland/Texas as lyophylized samples of purity GF (gel filtration). The concentrations of the oligonucleotides in solution were chosen so that the samples exhibited an absorption of $A = 2\ \mathrm{cm}^{-1}$ at 260 nm. Extinction coefficients at 260 nm were taken according to the specifications of the manufacturer. With typical values of about $0.75-1.5 \times 10^4$ L mol^{-1} cm^{-1} for the monomers and of about $5-20 \times 10^4$ L mol^{-1} cm^{-1} for sequences with 8−15 bases, typical concentrations were in the range of 10^{-5} M for the oligomers with $n > 8$ to 10^{-4} M for the monomers. Absorption was measured with a UV/vis double-path spectrometer (Kontron UVIKON 860), using the buffer as a reference. Static fluorescence was also recorded using a 150 W Xe high-pressure lamp in a Hitachi F4010 spectrometer.

Measurement, Calibration and Signal Evaluation Procedures. For a typical fluorescence measurement using the picosecond laser/streak camera setup, the emission of 3000 consecutive laser pulses was integrated, corresponding to a time period of 5 min for each experiment. From each measurement, a two-dimensional image was obtained with a time and a wavelength axis; intensities are stored with a 16-bit resolution by the CCD chip. The time and wavelength axes correspond to the selected spectrometer dispersion and streak interval; for most of the experiments, a wavelength range of 200 nm (300−500 nm) and a time interval 0−5 ns were chosen. The wavelength span and the absolute spectral position were determined using Rayleigh and Raman scattering with different excitation wavelengths between 250 and 350 nm; the Raman signature of water (Raman shift of 3450 cm^{-1}) was used as a reference in all images. Since the efficiency of the spectrograph grating (blaze 500 nm) and of the camera are not constant over this large wavelength region, a calibration was performed using a deuterium lamp and a halogen lamp with a blackbody temperature of 3200 K. For the polarization-sensitive experiments, the different reflection efficiency of the grating for horizontally and vertically polarized light was taken into account by determining independent calibration curves. To investigate potential damaging effects on the biomolecular samples by the irradiation of laser light, a series of experiments was conducted with attenuation of the laser beam. Also, measurements were performed repeatedly with the same sample. No indication of deterioration of the samples was found in any experiment.

Two-dimensional raw data images were processed by assigning the corresponding time and wavelength scales. Background luminescence was measured with the laser path blocked and subtracted from the fluorescence images. Furthermore, a smoothing procedure was used averaging information from 3 × 3 pixels. To account for the wavelength dependence of the detection efficiency, the images were divided by the appropriate calibration file, considering the respective polarization if necessary. For the evaluation of spectra and of temporal decays from the processed fluorescence images, cross sections were taken through the image, and either temporal or spectral range was kept constant. For temporal profiles, the spectral bandwidth was typically taken to be 5−10 nm. Fluorescence decays were evaluated using a biexponential fit

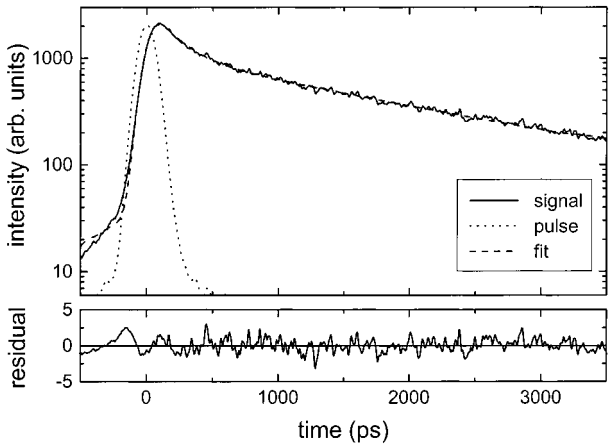

Figure 2. Time-resolved fluorescence decay curve for $d(A)_{15}$ at detection wavelength $\lambda_{em} = 400$ nm (solid), laser pulse (dotted), and fit to a biexponential model (dashed). The graph at the bottom is the weighted residual.

$$I(t) = \sum_{i=1}^{2} \alpha_i e^{-t/\tau_i} \tag{1}$$

Here, $I(t)$ is the time-dependent fluorescence intensity, and α_i is the amplitude corresponding to τ_i. The detected signal $F(t)$ results from a convolution of the fluorescence intensity $I(t)$ and the temporal profile of the exciting laser pulse, $P(t)$

$$F(t) = \int_0^t P(t')I(t-t')\,dt' = P(t) \otimes I(t) \tag{2}$$

In principle, the temporal decay of the fluorescence may be obtained by deconvolution. However, this procedure is of questionable success if the signal-to-noise level is nonnegligible. Therefore, we have used the method of numerical reconvolution. For this, the pulse profile $P(t)$ is convoluted with an estimated function, and the resulting $F(t)$ is iteratively fitted to the signal $I(t)$ by minimizing χ^2

$$\chi^2 = \sum_{i=1}^{x} \frac{(I(t_i) - F(t_i))^2}{\sigma_i^2} \tag{3}$$

with $I(t_i)$ being the individual data points. The standard deviation σ_i for each data point may be estimated from Poisson statistics with $\sigma_i = \sqrt{I(t_i)}$. For minimizing χ^2, the routine of Marquardt and Levenberg[43] is used. As a suitable criterion for the quality of the fit, the weighted residual $R(t)$ is determined according to

$$R(t_i) = \frac{I(t_i) - F(t_i)}{\sqrt{I(t_i)}} \tag{4}$$

A numerical fitting routine for multidimensional fluorescence data following[44] was employed. A typical time-resolved fluorescence signal is shown in Figure 2 together with the pulse profile and the biexponential fit. The lower trace shows the

weighted residual. Since this residual is unstructured, it can be concluded that this fit is sufficient to describe the observed fluorescence decay curves. In this case, two lifetimes of $\tau_1 = 1630 \pm 70$ ps and $\tau_2 = 170 \pm 30$ ps were deduced. Errors were determined with a rigorous error analysis[45] in a confidence interval of 97.7% (2σ).

Recently, Jasuja et al.[46] demonstrated that simple mono- and biexponential fits are not always adequate to describe the fluorescence spectra of complexes such as T4MPyP + GMP. Instead, they used fits to one continuous, Lorentzian-shaped distribution for the short and one single-exponential for the long lifetime component. However, tests for several of the fluorescence spectra evaluated for this paper showed that in our case the quality of the fit does not significantly improve by introducing Gaussian- or Lorentzian-shaped distributions. In many cases the opposite was true: due to the increasing number of free parameters the fit is not as stable as before and the accuracy generally drops. Additionally, it should be pointed out that numerical reconvolution is only one method to recover lifetimes from experimental spectra. Frequently, the maximum entropy method (MEM) is used,[47,48] which is supposed to be more stable and less affected by the initial parameters. However, for high-quality data both MEM and reconvolution techniques will yield the same results. A detailed comparison of these methods can be found in the work of Hof et al.[49]

For polarization-resolved measurements, the fluorescence anisotropy $r(t)$ was determined from the difference $D(t)$ of the detected intensities in parallel and vertical direction, $I_{||}(t)$ and $I_{\perp}(t)$ respectively, reduced by the total intensity $S(t)$

$$r(t) = \frac{I_{||}(t) - I_{\perp}(t)}{I_{||}(t) + 2I_{\perp}(t)} = \frac{D(t)}{S(t)} \tag{5}$$

The measured fluorescence decays for each polarization direction are also convoluted with the pulse profile. Therefore, the same numerical reconvolution routine as above is used to evaluate the time-dependent anisotropy from fits to the difference function $D_{exp}(t)$ and the intensity sum function $S_{exp}(t)$ with

$$S_{exp}(t) = P(t) \otimes S(t) = P(t) \otimes \sum_{i=1}^{n} \alpha_i e^{t/\tau_i} \tag{6}$$

$$D_{exp}(t) = P(t) \otimes D(t) = P(t) \otimes \sum_{j=1}^{n} \alpha_j e^{t/\tau_j} \tag{7}$$

It might be argued that more than two exponential decay functions might need to be considered for a valid description of the fluorescence behavior of DNA and other biomolecules. In previous work, single-exponential fits[41] as well as fits with four and more exponentials have been used,[16,50,51] and some authors[51,52] rely on the maximum entropy method.[53] In our study on oligonucleotides, we have been limited by the signal-to-noise level to extract more than two meaningful lifetime components. As a previously unachieved result, our method provides direct correlations between the temporal and spectral fluorescence behavior, which enables us to distinguish between monomer and excimer- or exciplex-related components. The application of multiexponential fit routines in our data evaluation is being examined.

Results and Discussion

As a first series of experiments, the contribution of monomer fluorescence and its importance in the fluorescence-time spectra of CMP and cytosine-derived oligonucleotides $d(C)_n$ with a sequence length of $n = 2-15$ were investigated. For this, absorption and static fluorescence spectra were analyzed first. The absorption wavelengths of 260 nm (CMP and $d(C)_2$) and 282 nm ($d(C)_{n>2}$) were used. The absorption spectra of monomer and dimer are quite similar, while the 15-mer exhibits a slightly enhanced absorption near 280−320 nm; absorption maxima coincide near 270 nm. While the static fluorescence spectra are also almost identical for the monomer and dimer,[36] the 15-mer fluorescence exhibits a red-shift, as described earlier for polyC[36] with a maximum near 400 nm; this was attributed to excimer formation.[36] Furthermore, a strong increase in the fluorescence intensity is noted with increasing sequence length, which is consistent with the increase in quantum yield from CMP to CpC reported earlier.[36]

In addition to the spectral emission investigated in previous work,[27,29,33,36] Figure 3 demonstrates the type and quality of information which may be obtained with the two-dimensional picosecond laser approach. The false-color images in Figure 3a−c give a striking impression of the differences in the fluorescence-time behavior between the monomer (a), the dimer (b), and the 15-mer (c). As a common feature, the Raman signal of H_2O is seen in all images at the upper left; it may be well distinguished from the fluorescence signal and serve as a time and wavelength reference as well as an indicator for changes in the laser energy. The monomer fluorescence shown in Figure 3a exhibits a short lifetime and a maximum near 330 nm, as seen in the static spectra. As may be discerned already at first glance, the oligomers $d(C)_n$ with $n = 2$, 15 (Figure 3b,c) show an additional fluorescence component at longer wavelength, which is associated with a significantly longer lifetime. In Figure 4, the time dependence of the fluorescence signal of $d(C)_{15}$ is shown at 340, 400, and 460 nm; these decay curves correspond to vertical cross sections of the two-dimensional image in Figure 3c. Although intrinsic fluorescence of these oligonucleotides has, to our knowledge, not been investigated before at these quite low concentrations (10 μM), the signal-to-noise-level is quite satisfactory.

The two-dimensional fluorescence images for the complete series of monomers and oligomers with $n = 2-15$ were evaluated as described above by performing biexponential fits to the fluorescence decays as a function of wavelength; cross sections were taken with 20 nm increments. Two processes were distinguished with a long decay time (τ_1) and a shorter component (τ_2). The results are displayed in part a and b of Figure 5, respectively. A significant difference is seen between the long lifetime component of the monomer (about 500 ps at 380−400 nm) and those of the oligomers (about 1200 ps at 380−400 nm). Also, compared with the monomer fluorescence, a much more important increase in the long lifetime component with wavelength in the range of 340−460 nm is observed for the oligomers. Values for τ_1 are almost independent of sequence length for $n = 2-15$ (Figure 5a). The shorter lifetime component τ_2, in contrast, depends both on wavelength and on sequence length; for the monomer, it is almost constant at values below 40 ps and corresponds to the time resolution of the apparatus.

Not only the lifetimes, but also the fluorescence intensities associated with τ_1 and τ_2 are quite different for the monomer on one hand and the oligonucleotides on the other. The sum of the intensities of the long- and short-lived decay components from the time-resolved spectra agrees excellently with those of the static fluorescence measurements (Figure 6, top left); however, additional information is obtained on the relative importance of the different processes contributing to the

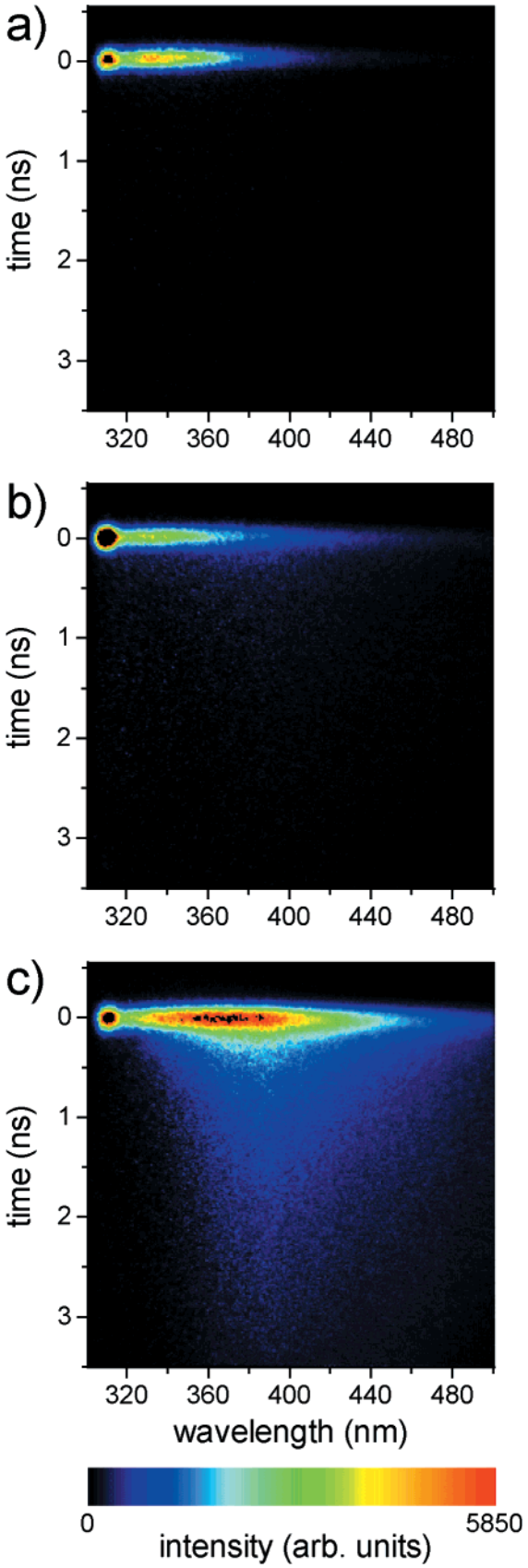

Figure 3. Simultaneous time- and wavelength-resolved measurements of the fluorescence intensity for (a) CMP, (b) $d(C)_2$, and (c) $d(C)_{15}$. Intensities are given in a false-color representation.

measured spectra and lifetimes. For the CMP monomer, the long-lived process contributes less than 10% to the fluorescence

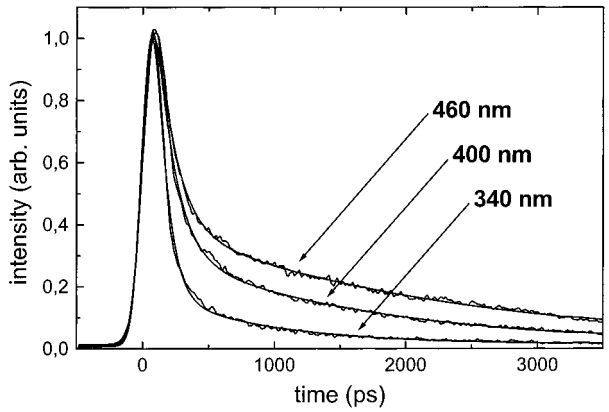

Figure 4. Normalized time-resolved fluorescence decay curves for $d(C)_{15}$ at three different detection wavelengths. These curves correspond to vertical cross sections through Figure 3c.

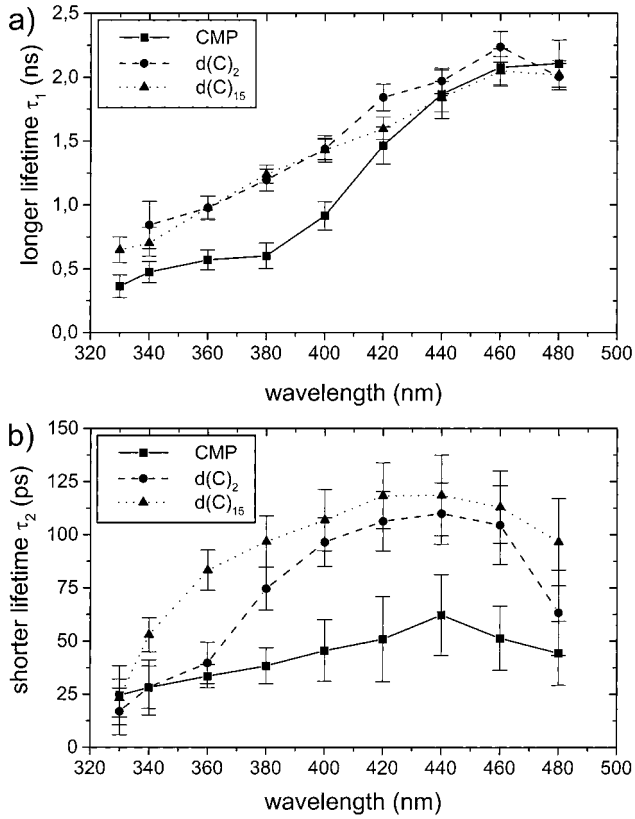

Figure 5. Comparison of the wavelength dependence of the fitted fluorescence lifetimes for CMP, $d(C)_2$, and $d(C)_{15}$: (a) long component and (b) short component.

intensity at 320−340 nm (the region where the fluorescence is highest) as seen in Figure 6, bottom left. Only at very high wavelengths (λ > 440 nm) does it contribute to more than 50%. However, the total fluorescence intensity is already very low in this region, so the contribution of the long-lived process to the total fluorescence yield is negligible in this case. In contrast, for the oligomers the intensity of the long-lived process always dominates at λ > 370 nm. Since the fluorescence spectra of the oligomers are red-shifted (λ_{max} = 385 nm for $d(C)_{15}$), the major part of the fluorescence is due to the long-lived process.

In comparison with earlier work at 80 and 300 K,[27,33,36] it may be assumed that the long-wavelength fluorescence components τ_1 arise from excimer formation; lifetimes for such emissions were postulated to be in the nanosecond regime,[54] in agreement with those observed here. It might be assumed that

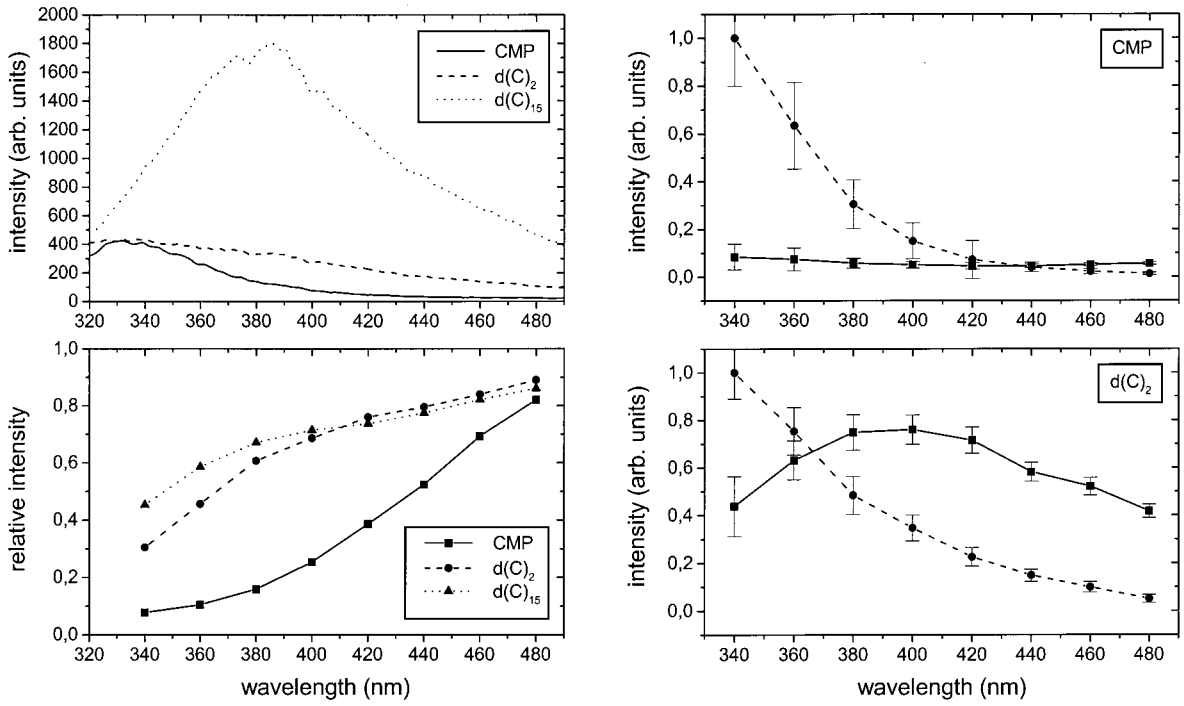

Figure 6. Total fluorescence yield (top left) and contribution of the intensity associated with the longer fluorescence lifetime to the total fluorescence (bottom left) for CMP, $d(C)_2$, and $d(C)_{15}$. On the right, decay-associated spectra for CMP and $d(C)_2$ are shown (solid line, contribution of the process with longer lifetime; broken line, contribution of the process with shorter lifetime).

the short-lived component τ_2 would correspond to the monomer fluorescence decay. Fluorescence lifetimes of the DNA bases have recently been determined by Häupl et al.[41] and are with a few picoseconds much shorter than the temporal resolution of this experiment. A direct comparison with the lifetime of cytosine of 2.2 ± 0.5 ps obtained in their work is thus not possible. For the dimer and oligomers, τ_2 at 340 nm increases to about 80 ps for $d(C)_{15}$, a value which may be accurately resolved with our apparatus (Figure 5b). It may be speculated that these differences in τ_2 might be a consequence of different exposure of the bases to the solvent in these oligonucleotides with variable length. The excimer fluorescence, however, seems less sensitive to such processes, since τ_1 does not change with $n = 2-15$. Interestingly, a long-lived process is also observed for the monomer (compare Figure 5a), even though the relative intensity is very low in this case (Figure 6). This could be due to excimers forming in collisions where one molecule is in the ground state and one in an excited state, a process which would occur with low probability and thus contribute only marginally to the observed fluorescence signal.

As a next step, dynamic fluorescence spectra of homo-oligonucleotides with identical chain length but different bases are compared. Figure 7 shows the wavelength-dependence of the longer fluorescence lifetime for $d(A)_{15}$, $d(C)_{15}$, $d(G)_{15}$, and $d(T)_{15}$. For all four systems, the same general trend is observed: at short wavelengths, the longer lifetime is in all cases shorter than 1 ns; after that, τ_1 gradually increases. For $d(T)_{15}$, the lifetime remains more or less constant with $\tau_1 \approx 1.2$ ns for wavelengths larger than 360 ns. For $d(G)_{15}$, the relaxation time is less than 1 ns for all wavelengths. In contrast, the longer lifetime reaches distinct maxima close to 2 ns for $d(A)_{15}$ and $d(C)_{15}$. Figure 8 shows the intensity associated with the two lifetimes for the same oligonucleotides. The spectra are normalized to 1 to facilitate comparison of the trends; the absolute intensity is highest for $d(A)_{15}$ (three times as high as $d(G)_{15}$), whereas $d(C)_{15}$ and $d(T)_{15}$ have comparable fluorescence intensities (roughly 30% less than of $d(G)_{15}$). Here, very

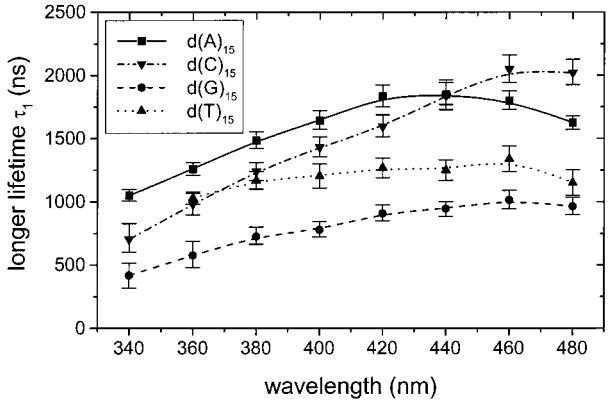

Figure 7. Wavelength-dependence of the longer fluorescence lifetime for homo-oligonucleotides with identical chain length ($d(A)_{15}$, $d(C)_{15}$, $d(G)_{15}$, $d(T)_{15}$).

pronounced structures are observed. For $d(A)_{15}$, the contribution of the process with the short lifetime to the total fluorescence is highest at $\lambda = 360$ nm, but well below 25% over the complete wavelength range. The process with the long lifetime, which is associated with the excimer-fluorescence, is strongest around $\lambda = 400$ nm and completely dominates the spectrum. This also corresponds to the maximum intensity in the time-integrated spectra (Figure 6a). Cytosine has a similar, but somewhat weaker, tendency to form excimers. For $d(C)_{15}$, the short-lived process dominates for wavelengths below 360 nm. However, the peak in the fluorescence spectra around 400 nm is clearly due to the process with long lifetime. In contrast, the oligonucleotides $d(G)_{15}$ and $d(T)_{15}$ show a completely different pattern. Here, the strongest fluorescence is always found at short wavelengths, and it can be attributed to monomer fluorescence by its short lifetime. In both cases, the intensity of the long-lived process peaks at $\lambda = 400$ nm. For both $d(G)_{15}$ and $d(T)_{15}$, the contribution of excimers to the total fluorescence yield is well below 50%, whereas it is 67% for $d(C)_{15}$ and more than 81% for $d(A)_{15}$.

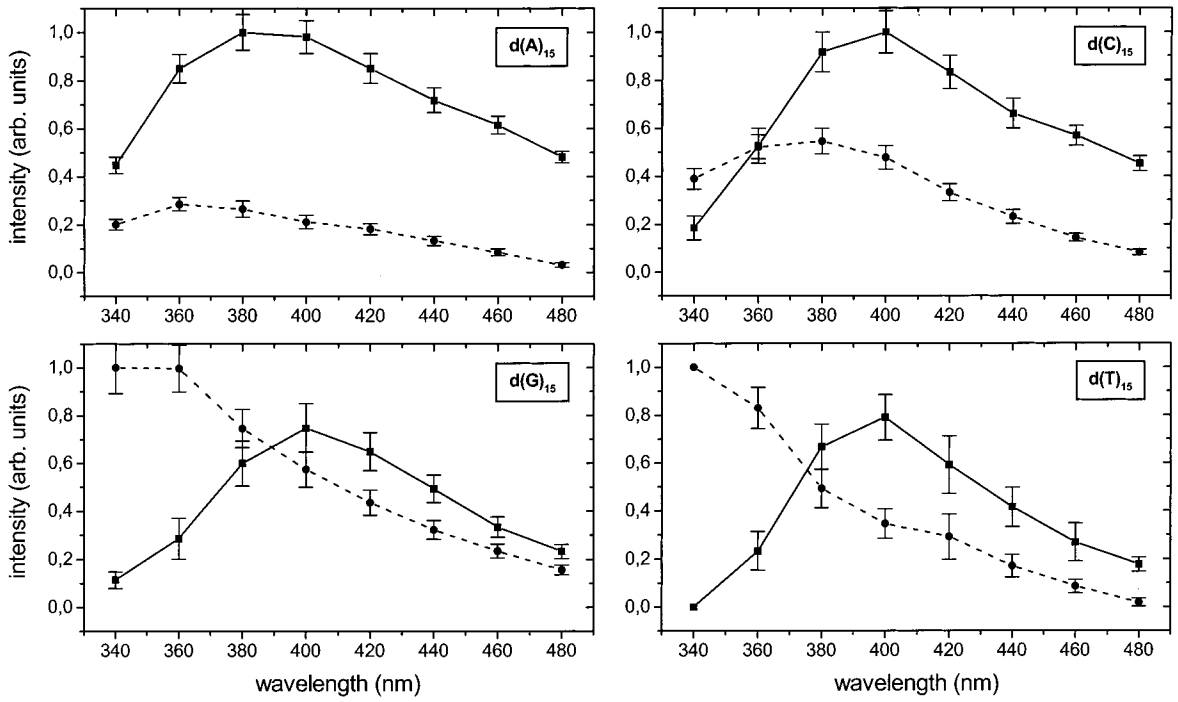

Figure 8. Intensity associated with the two lifetimes for homo-oligonucleotides with identical chain length ($d(A)_{15}$, $d(C)_{15}$, $d(G)_{15}$, $d(T)_{15}$). Maximum intensity normalized to 1.0 to facilitate comparison of the spectra. Solid line, contribution of the process with longer lifetime; broken line, contribution of the process with shorter lifetime.

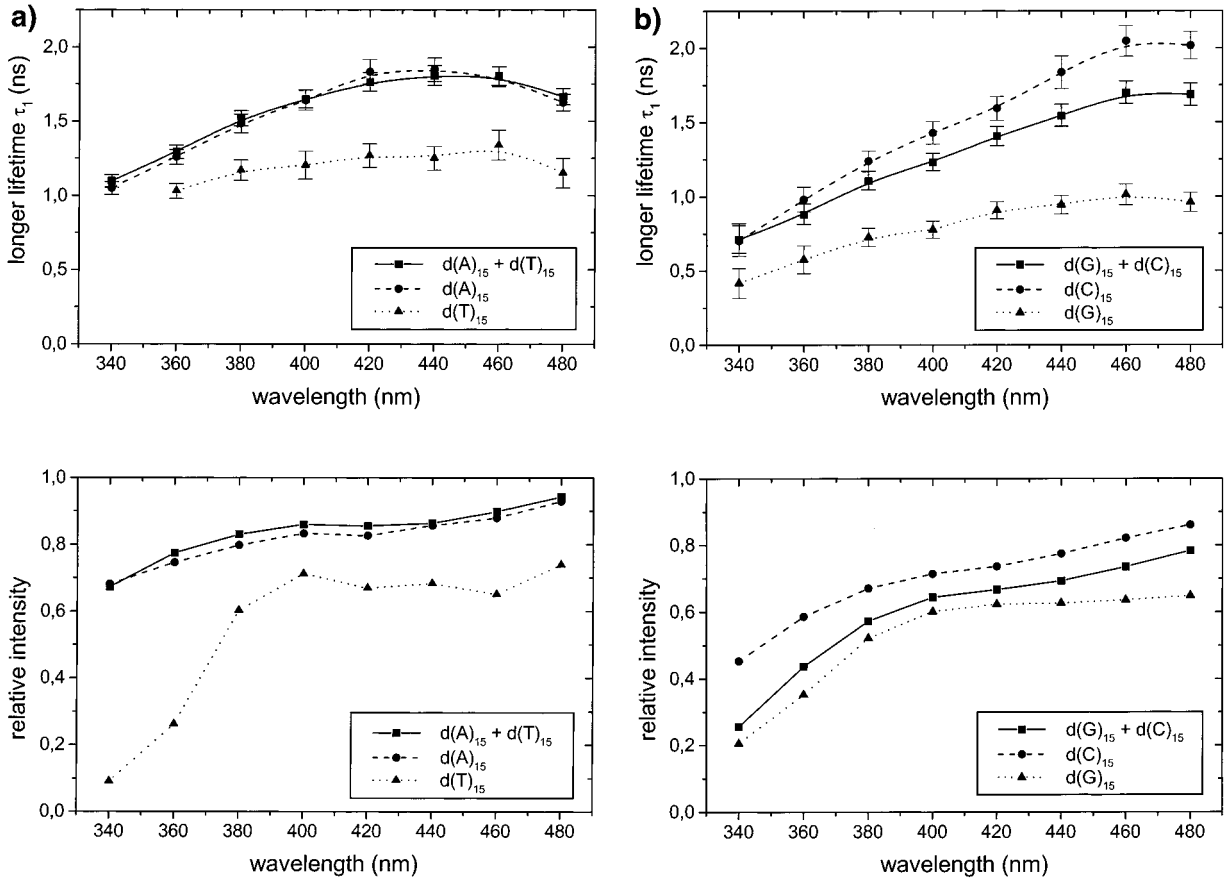

Figure 9. Wavelength-dependence of the longer lifetime (top) and of the associated relative intensity (bottom) for homo-oligonucleotides and in equimolar mixtures (where double helices form): (a) $d(A)_{15}$ and $d(T)_{15}$ and (b) $d(C)_{15}$ and $d(G)_{15}$.

In Figure 9, the wavelength-dependence of the longer lifetime and of the associated relative intensity for single-stranded homo-oligonucleotides and in equimolar mixtures (where double helices form) is shown. For a mixture of $d(A)_{15}$ and $d(T)_{15}$, the spectrum is completely dominated by the strong adenine excimer fluorescence. Both the lifetime of the long-lived process and its contribution to the fluorescence at a given wavelength (Figure 9a) are identical within the error margins to that of the pure $d(A)_{15}$. For the mixture of guanine and cytosine, a different behavior is observed, since both have comparable fluorescence

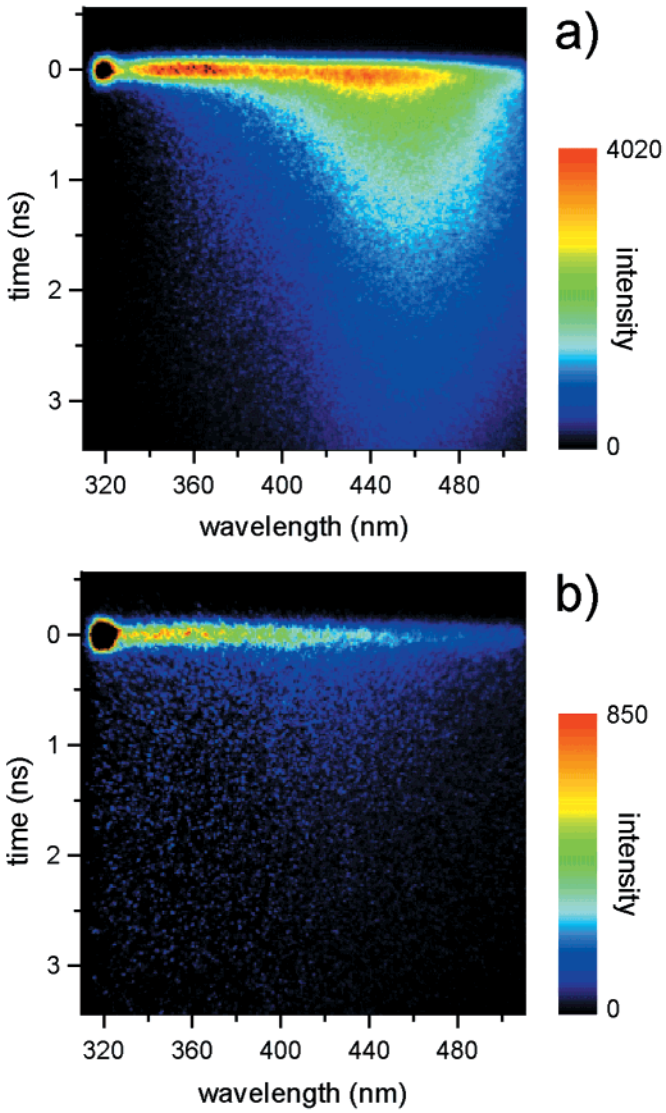

Figure 10. Simultaneous time- and wavelength resolved measurements of the fluorescence intensity for self-complementary oligonucleotides: (a) $d(AT)_8$ and (b) $d(GC)_8$.

yields. The lifetime of the long-lived process as well as its relative intensity is close to the mean of the values for the pure oligonucleotides $d(C)_{15}$ and $d(G)_{15}$ (Figure 9b). As a consequence, it may be concluded that strong excimer fluorescence of the respective bases is found not only in single-stranded but also in double-helical DNA-oligonucleotides. The more rigid distance and the angle between the individual bases have only a negligible influence on strength and wavelength dependence of the excimer fluorescence. Additionally, it should be noted that we observe strong AA* excimer fluorescence for both single-stranded and double-helical oligonucleotides. This result is in contrast to that published by Ge et al.[55] in an earlier paper, who claimed that in polydA×polydT oligonucleotides only nonfluorescent AA* excimers are formed.

Simultaneous time- and wavelength-resolved measurements of the fluorescence intensity for self-complementary oligonucleotides are shown in Figure 10 in a false-color representation. Large differences between the fluorescence patterns are readily visible: Whereas $d(AT)_8$ exhibits very strong fluorescence, especially at long wavelengths, the spectrum of $d(GC)_8$ is dominated by the Raman peak at 314 nm and has a markedly lower intensity than that of pure cytosine (Figure 3) or guanine. Figure 11 shows a more detailed analysis of these two images. For $d(AT)_8$, the value of the longer fluorescence lifetime first decreases slightly from 1.4 ns at 340 nm to 1.3 ns at 380 nm and then rises sharply to values close to 2 ns at the long-wavelength part of the spectrum. This trend is completely different from that of the homo-oligonucleotides $d(A)_{15}$ and $d(T)_{15}$, which are plotted for comparison. The intensity distribution (Figure 11a, bottom) shows equally large differences: Whereas the strong $d(A)_n$ excimer fluorescence peaks around 380 nm (Figure 8), the spectrum of $d(AT)_8$ is dominated completely by long-lived fluorescence (87% of the integrated yield), which exhibits its maximum around $\lambda = 460$ nm. Both, the long lifetime and the large red-shift are indicatives that exciplexes are responsible for the fluorescence.

The other self-complementary oligonucleotide $d(GC)_8$ exhibits a different fluorescence pattern. Here, the intensity is much lower than that of the pure homo-oligonucleotides with identical chain length (by a factor of 3 in comparison with $d(C)_{15}$ and 5 for $d(G)_{15}$) and is even lower than that of the monomers (see Figures 3 and 10). This indicates strong quenching of GC base pairs, which has also been observed by other groups at low temperatures.[26] In Figure 11b we have attempted a more detailed analysis of the remaining fluorescence. The lifetime τ_1 starts at 1.6 ns for short wavelengths, then drops to 1.0 ns at 400 nm and remains almost constant towards longer wavelengths. This trend is markedly different than that of both pure cytosine and pure guanine and thus indicates that the individual monomer fluorescence is not responsible for the residual fluorescence in $d(GC)_8$. This observation and the high contribution of the process with longer lifetime at $\lambda = 420$ nm (Figure 11b, bottom) hint that weak exciplex fluorescence might be the origin. However, the low intensity and the associated relatively large error bars on the fitted lifetimes and intensities prevent a conclusive attribution of the process responsible for this fluorescence.

To facilitate the comparison of the different oligonucleotides, the results of the fluorescence lifetime analysis of CMP, $d(C)_2$, $d(C)_{15}$, $d(A)_{15}$, $d(G)_{15}$, $d(T)_{15}$, $d(AT)_8$, and $d(GC)_8$ are summarized in Table 1 for three different emission wavelengths.

The measurements described above have been obtained by integrating all fluorescence photons regardless of their polarization properties. However, additional information may be obtained by detecting fluorescence with the electrical field vector parallel and vertical to the exciting laser beam separately (refer to Figure 1 for the definition of the polarization vectors). In Figure 12, the time-resolved decay curves for vertical and parallel signal polarization as well as their difference are shown for $d(A)_{15}$. It can be seen that close to the excitation pulse fluorescence polarized parallel is markedly stronger than the vertical component, whereas the intensities are nearly identical for times larger than 1 ns. From these curves, the fluorescence anisotropy is calculated using eq 5. Examples are shown in the bottom part of Figure 12 for $d(A)_2$ and $d(A)_{15}$. For both oligonucleotides an initial signal anisotropy of $r(0) \approx 0.2$ is observed. For $d(A)_2$, the anisotropy decreases monoexponentially with a relaxation time of $\tau = 101$ ps, whereas a biexponential model with decay times of $\tau_1 = 96$ ps and $\tau_2 = 480$ ps was necessary to adequately describe the curve observed for $d(A)_{15}$. Here, the short relaxation time may be attributed to local movements of the individual bases,[3,56] whereas the longer lifetime is most likely due to physical movement (e.g. a rotation) of the complete oligonucleotide. These results compare favorably with that obtained by Guest et al.[3] and Georghiou et al.[57] for double-helical DNA. Time-resolved anisotropy measurements can thus be used to determine the size of the oligonucleotide in solution (the larger the τ_2 value, the larger the diameter)

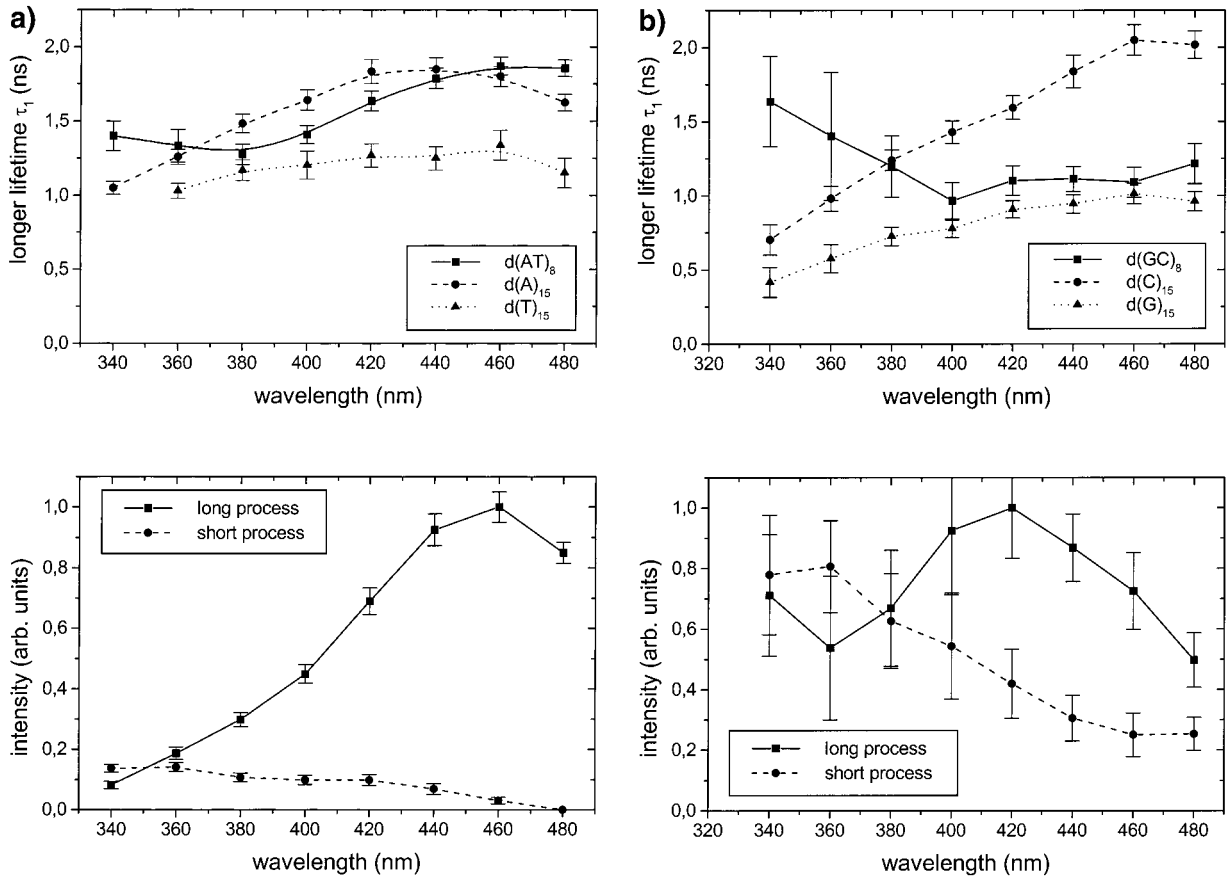

Figure 11. Comparison of the wavelength-dependence of the longer lifetime (top) and the associated intensity (bottom) for (a) $d(AT)_8$, $d(A)_{15}$, and $d(T)_{15}$ and (b) $d(GC)_8$, $d(G)_{15}$, and $d(C)_{15}$.

TABLE 1: Time-Resolved Fluorescence Decay Parameters of All Samples for Three Different Emissions Wavelengths[a]

	$\lambda_{em} = 340$ nm				$\lambda_{em} = 400$ nm				$\lambda_{em} = 460$ nm			
sample	I_1 (10^{-2})	τ_1 (ps)	I_2 (10^{-2})	τ_2 (ps)	I_1 (10^{-2})	τ_1 (ps)	I_2 (10^{-2})	τ_2 (ps)	I_1 (10^{-2})	τ_1 (ps)	I_2 (10^{-2})	τ_2 (ps)
CMP	8	480	100	30	5	920	15	50	5	2080	2	50
$d(C)_2$	44	840	100	30	76	1440	35	100	52	2240	10	100
$d(C)_{15}$	19	700	39	50	100	1430	48	110	57	2050	14	110
$d(A)_{15}$	45	1050	20	150	98	1640	21	240	61	1800	8	260
$d(G)_{15}$	11	420	100	80	75	780	57	120	33	1010	23	150
$d(T)_{15}$			100	40	79	1200	35	110	27	1340	9	270
$d(AT)_8$	8	1400	14	90	45	1410	10	170	100	1870	3	230
$d(GC)_8$	71	1640	78	60	92	970	54	140	72	1090	25	160

[a] $I_i(\lambda_{em}) = [\alpha_i(\lambda_{em})\tau_i(\lambda_{em})]/I_{max}(\lambda_{em})$.

and allow one to distinguish different conformations. However, at present our database is not yet large enough to allow a systematic study of these effects.

Summary

The intrinsic fluorescence of oligonucleotides has been investigated using picosecond excitation with a regeneratively amplified, frequency-tripled output of a Ti:sapphire laser as the light source. Signals have been detected with a streak camera located in the exit plane of a spectrograph. This approach yields simultaneous time- and wavelength-resolved information and thus facilitates the assignment of the observed signals to different photophysical processes. Fluorescence decay curves extracted from these two-dimensional images have been fitted to the model of biexponential decay using a numerical reconvolution technique; agreement was good in all cases investigated. The fitting procedure allowed the resolution of lifetimes down to 20 ps.

Comparison of time-resolved spectra of all four bases with different chain lengths allows the identification of different processes contributing to the fluorescence: in all cases, monomer fluorescence is strongest at short wavelengths and exhibits a rapid decay with a decay time close to, or below, our experimental resolution. In contrast, at longer wavelengths a process with a lifetime close to 2 ns tends to dominate (with a maximum around $\lambda_{max} = 400$ nm). This process is most likely due to excimer fluorescence.

Fluorescence from $d(A)_n$ is comparatively strong and mainly due to excimers (both, in single-stranded and double-helix conformation). $d(C)_n$ has a similar, but weaker tendency to form radiative excimers, whereas the fluorescence spectra of the oligonucleotides $d(G)_n$ and $d(T)_n$ is dominated by momomer fluorescence. Measurements in equimolar mixtures of the complementary homo-oligonucleotides show that the conformation (single-strand or double-helix) has only a negligible influence on the strength and the spectral form of the excimer fluorescence.

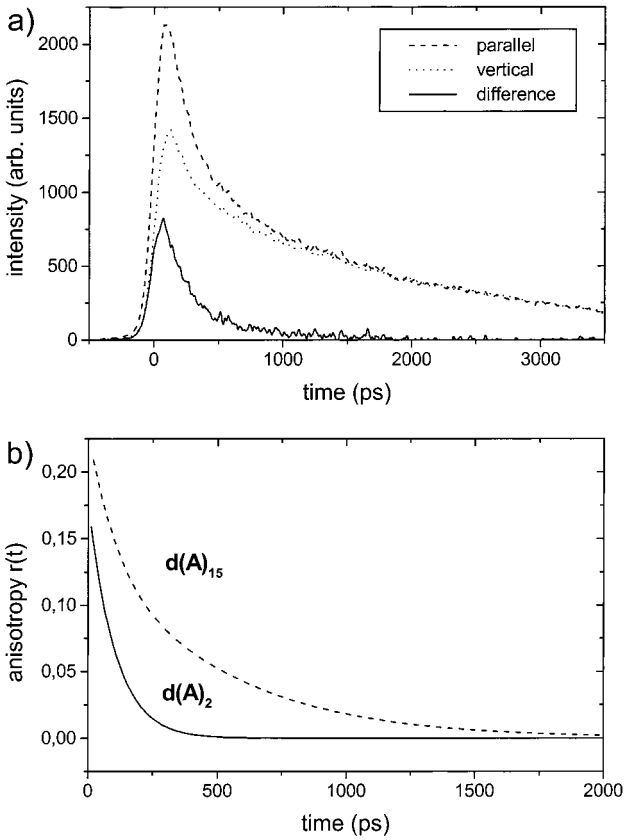

Figure 12. Fluorescence anisotropy measurements for an emission wavelength $\lambda_{em} = 400$ nm: (a) time-resolved decay curves for vertical and parallel signal polarization and their difference (for $d(A)_{15}$) and (b) the calculated signal anisotropy for $d(A)_2$ and $d(A)_{15}$.

For the self-complementary oligonucleotide $d(AT)_8$, the fluorescence maximum is markedly red-shifted ($\lambda_{max} = 460$ nm). At the location of the strongest fluorescence, nearly all the intensity is due to a process with a long lifetime ($\tau = 1.9$ ns), which is identified as exciplex fluorescence. In contrast, fluorescence from $d(GC)_8$ is very weak, much less than that of pure guanine or cytosine. These two bases efficiently quench their respective fluorescence. In conclusion, we thus expect AA* and AT* exciplexes to be the dominant origin for fluorescence of naturally occurring DNA.

Finally, we present first simultaneous time-, wavelength-, and polarization-resolved measurements. The observed anisotropy decay curves show one rapid process with a lifetime around 100 ps, which can be attributed to local movements of the individual bases, whereas the longer relaxation time depends on the size of the oligonucleotide and corresponds to physical movement (e.g. a rotation) of the complete molecule.

Acknowledgment. Assistance of B.-L. Marg at the first measurements is gratefully acknowledged.

References and Notes

(1) Georghiou, S.; Bradrick, T. D.; Philippetis, A.; Beechem, J. M. *Biophys. J.* **1996**, *70*, 1909.
(2) Cain, R. J.; Click, G. D. *Nucleic Acids Res.* **1997**, *25*, 836.
(3) Guest, C. R.; Hochstrasser, R. A.; Sowers, L. C.; Millar, D. P. *Biochemistry* **1991**, *30*, 3271.
(4) Winter, S.; Kirschstein, S.; Lober, G. *Nucleosides Nucleotides* **1997**, *16*, 531.
(5) Genest, D.; Wahl, P. *Biochim. Biophys. Acta* **1978**, *521*, 502.
(6) Collini, M.; Chirico, G.; Baldini, G.; Bianchi, M. E. *Macromolecules* **1998**, *31*, 695.
(7) Barone, F.; Chirico, G.; Matzeu, M.; Mazzei, F.; Pedone, F. *Eur. Biophys. J.* **1998**, *27*, 137.
(8) Manoharan, M.; Tivel, K. L.; Zhao, M.; Nafisi, K.; Netzel, T. L. *J. Phys. Chem.* **1995**, *99*, 17461.
(9) Yguerabide, J.; Talavera, E.; Alvarez, J. M.; Afkir, M. *Anal. Biochem.* **1996**, *241*, 238.
(10) Kumke, M. U.; Li. G.; McGown, L. B.; Walker, G. T.; Linn, C. P. *Anal. Chem.* **1995**, *67*, 3945.
(11) Ellouze, C.; Piot, F.; Takahashi, M. *J. Biochem.* **1997**, *121*, 521.
(12) Vámosi, G.; Gohlke, C.; Clegg, R. M. *Biophys. J.* **1996**, *71*, 972.
(13) Müller, R.; Herten, D. P.; Lieberwirth, U.; Neumann, M.; Sauer, M.; Schulz, A.; Siebert, S.; Drexhage, K. H.; Wolfrum, J. *Chem. Phys. Lett.* **1997**, *279*, 282.
(14) Nunnally, B. K.; He, H.; Li, L. C.; Tucker, S. A.; McGown, L. B. *Anal. Chem.* **1997**, *69*, 2392.
(15) Hawkins, M. E.; Pfleiderer, W.; Balis, F. M.; Porter, D.; Knutson, J. R. *Anal. Biochem.* **1997**, *244*, 86.
(16) Lakowicz, J. R.; Gryczynski, I.; Malak, H.; Schrader, M.; Engelhardt, P.; Kano, H.; Hell, S. W. *Biophys. J.* **1997**, *72*, 567.
(17) Dunkak, K. S.; Otto, M. R.; Beechem, J. M. *Anal. Biochem.* **1996**, *243*, 234.
(18) Buist, A. H.; Muller, M.; Gijsbers, E. J.; Brakenhoff, G. J.; Sosnowski, T. S.; Norris, T. B.; Squier, J. *J. Microsc. Oxford* **1997**, *186*, 212.
(19) Li, L. C.; He, H.; Nunnally, B. K.; McGown, L. B. *J. Chromatogr. B* **1997**, *695*, 85.
(20) Deka, C.; Steinkamp, J. A. *Appl. Opt.* **1996**, *35*, 4481.
(21) Keji, J. F.; Bell-Prince, C.; Steinkamp, J. A. *Cytometry* **1999**, *35*, 48.
(22) Carlsson, C.; Larsson, A.; Björkman, M.; Jonsson, M.; Albinsson, B. *Biopolymers* **1997**, *41*, 481.
(23) Broo, A. *J. Phys. Chem. A* **1998**, *102*, 526.
(24) Ye, J. Y.; Yamauchi, M.; Yogi, O.; Ishikawa, M. *J. Phys. Chem.* **1999**, *103*, 2812.
(25) Albinsson, B. *J. Am. Chem. Soc.* **1997**, *119*, 6369.
(26) Eisinger, J.; Guéron, M.; Shulman, R. G.; Yamane, T. *Proc. Natl. Acad. Sci.* **1966**, *55*, 1015.
(27) Eisinger, J.; Shulman, R. G. *Science* **1968**, *161*, 1311.
(28) Aoki, T. I.; Callis, P. R. *Chem. Phys. Lett.* **1982**, *92*, 327.
(29) Callis, P. R. *Annu. Rev. Phys. Chem.* **1983**, *34*, 329.
(30) Görner, H. J. *Photochem. Photobiol. B* **1994**, *26*, 117.
(31) Nikogosyan, D. N.; Angelov, D.; Soep, B.; Lindqvist, L. *Chem. Phys. Lett.* **1996**, *252*, 322.
(32) Guéron, M.; Shulman, R. G.; Eisinger, J. *Proc. Natl. Acad. Sci.* **1966**, *56*, 814.
(33) Guéron, M.; Eisinger, J.; Shulman, R. G. *J. Chem. Phys.* **1967**, *47*, 4077.
(34) Wilson, R. W.; Morgan, J. P.; Callis, P. R. *Chem. Phys. Lett.* **1975**, *36*, 618.
(35) Hauswirth, W.; Daniels, M. *Photochem. Photobiol.* **1971**, *13*, 157.
(36) Vigny, P.; Favre, A. *Photochem. Photobiol.* **1974**, *20*, 345.
(37) Morgan, J. P.; Daniels, M. *Photochem. Photobiol.* **1980**, *31*, 101.
(38) Morgan, J. P.; Daniels, M. *Photochem. Photobiol.* **1980**, *31*, 207.
(39) Wilson, R. W.; Callis, P. R. *Photochem. Photobiol.* **1980**, *31*, 323.
(40) Kobayashi, S.; Yamashita, M.; Sato, T.; Muramatsu, S. *IEEE J. Quantum Electron.* **1984**, *QE−20*, 1383.
(41) Häupl, T.; Windolph, C.; Jochum, T.; Brede, O.; Hermann, R. *Chem. Phys. Lett.* **1997**, *280*, 520.
(42) Reuther, A.; Nikogosyan, D. N.; Laubereau, A. *J. Phys. Chem.* **1996**, *100*, 5570.
(43) Press, W. H.; Flannery, B. P.; Teukolsky, S. A.; Vetterling, W. T. *Numerical Recipes in C*; Cambridge University Press: Cambridge, 1988.
(44) Lakowicz, J. R. *Topics in Fluorescence Spectroscopy*; Plenum Press: New York, 1991; vol. 2: Principles.
(45) Brand, L. Numerical Computer Methods. In *Methods in Enzymology*; Academic Press: New York, 1992; pp 36−54.
(46) Jasuja, R.; Jameson, D. M.; Nishijo, C. K.; Larsen, R. W. *J. Phys. Chem. B* **1997**, *101*, 1444.
(47) Hof, M. *Biochim. Biophys. Acta* **1998**, *1388*, 143.
(48) Dijkstra, D. S.; Broos, J.; Visser, A. J. W.; van Hoek, A.; Robillard, G. T. *Biochemistry* **1997**, *36*, 4860.
(49) Hof, M.; Fleming, G. R.; Fidler, V. *Proteins Struct. Func. Genet.* **1996**, *24*, 485.
(50) Roy, M.; Periasamy, N. *Photochem. Photobiol.* **1995**, *61*, 292.
(51) Vincent, M.; Gallay, J.; Demchenko, A. P. *J. Phys. Chem.* **1995**, *99*, 14931.
(52) Das, T. K.; Mazumdar, S. *J. Phys. Chem.* **1995**, *99*, 13283.
(53) Livesey, A. K.; Brochon, A. K. *Biophys. J.* **1987**, *52*, 693.
(54) Eisinger, J. *Photochem. Photobiol.* **1968**, *7*, 597.
(55) Ge, G.; Georghiou, S. *Photochem. Photobiol.* **1991**, *54*, 301; Ge, G.; Georghiou, S. *Photochem. Photobiol.* **1991**, *54*, 477.
(56) Georghiou, S.; Kubala, S. M.; Large, C. C. *Photochem. Photobiol.* **1998**, *67*, 526.